Thermochemical Aspects of Superknock Development in IC Engines

Minh Bau Luong[1], Efstathios-Al. Tingas[2], and Hong G. Im[1]

[1]Clean Combustion Research Center, King Abdullah University of Science and Technology, Thuwal 23955-6900, Saudi Arabia
[2]School of Engineering and the Built Environment, Edinburgh Napier University, Edinburgh EH10 5DT, United Kingdom

1 Introduction

Downsized and boosted technologies in modern combustion engines provides higher thermal efficiency and cleaner combustion compared with the conventional IC engines. However, these engines operated under extreme conditions of high load and elevated pressure induce a higher possibility of abnormal preignition. Preignition is usually triggered by a premature auto-ignition induced by hot spots that occurs much earlier than spark timing, leading to higher temperature and pressure rise, and thus higher knock intensity, and even super-knock phenomena [1–6]. Super-knock is characterized by excessive pressure oscillations and extremely high pressure spikes in a few hundred bar that may lead to mechanical failure. The mechanism and the source of such irregular preignition events are still not well understood [7].

Zeldovich [8] provided a theoretical framework to classify different ignition regimes that relies on the speed of a spontaneous ignition front, S_{sp}, relative to the deflagration front, S_L, and sound speed, a. A successive ignition events in the presence of spatial reactivity gradients is determined through the spatial gradient of the ignition delay time, $S_{sp} = |\nabla \tau_{ig}|^{-1}$. Gu and Bradley [9] further mapped five different propagation modes into a regime diagram constructed upon two key non-dimensional parameters, $\xi = a/S_{sp}$ and $\varepsilon = (r_{hs}/a)/\tau_e$. ε is defined as the ratio of the residence time, r_{hs}/a, of the acoustic wave within the hot spot with a radius, r_{hs}, to the excitation time, τ_e, in which most of the chemical energy is released.

The different modes of ignition front propagation within a hot spot were identified primarily based on the initial state of the mixture conditions. However, a general finding of the previous studies [1–4, 7, 10–12] on superknock development is that once superknock triggered by localized hot spots, the subsequent development of premature auto-ignition process depends strongly on the thermochemical bulk mixture properties and the levels of inhomogeneities in temperature and composition. The relative contribution of thermochemical properties such as chemical kinetics, diffusion, and convection leads to the superknock development is still unknown. To this end, the objective of this study is to elucidate the thermochemical aspects of superknock development process by performing computational singular perturbation (CSP) and tangential stretching rate (TSR) analysis.

2   Theoretical framework of computational singular perturbation (CSP) and tangential stretching rate (TSR)

The species and energy equations that govern the evolution of a reactive-transport system can be cast in the general form of Eq. 1:

$$\frac{\partial \boldsymbol{z}}{\partial t} = \boldsymbol{L}(\boldsymbol{z}) + \boldsymbol{g}(\boldsymbol{z}) \tag{1}$$

where $\mathbf{g}(\mathbf{z})$ is the chemical source term of the system, $\mathbf{L}(\mathbf{z})$ is a spatial differential operator (convection and/or diffusion), $\mathbf{z}$ is the (N+1)-dimensional state column vector including the N species' mass fractions and temperature. Based on the CSP methodology [13], the system of Eq. 1 can be decomposed into the following form by using the CSP basis vectors α_i ($i = 1, N + 1$):

$$\frac{\partial \boldsymbol{z}}{\partial t} = \sum_{i=1}^{N+1} \boldsymbol{\alpha_i}(\boldsymbol{z}) h^i(\boldsymbol{z}) \tag{2}$$

where $h^i = \boldsymbol{b^i}(\boldsymbol{L}(\boldsymbol{z}) + \boldsymbol{g}(\boldsymbol{z}))$ is the amplitude of the i-th mode and $\boldsymbol{b^i}$ denotes the dual basis vector [13]. When M of these modes become exhausted the system evolves under the action of the remaining $N + 1 - M$ active/slow ones. Each mode is a mathematical quantity, characterized by an amplitude and a timescale. The first describes the impact of the associated mode to the system's slow evolution for the slow modes, while for the exhausted ones it describes the equilibrations that constrain the system's slow evolution on the slow manifold. The timescale describes the timeframe of action of the associated CSP mode. The CSP basis vectors $\boldsymbol{a_i}$ and covectors $\boldsymbol{b^i}$ ($i = 1, N + 1$) can be approximated to leading order, by the right and left, respectively, eigenvectors of the Jacobian $\boldsymbol{J}_g$ of $\boldsymbol{g}(\boldsymbol{z})$ [13, 14]. Depending on the sign of the associated eigenvalue, each mode is characterized as dissipative or explosive; the first are associated with negative eigenvalues while the latter are linked to positive eigenvalues. Explosive modes tend to drive the system away from equilibrium, hence are associated with limit phenomena such as ignition, flame front etc. [15,16]. However, the mere presence of an explosive mode is not an indicator for their dominance against the rest of the modes. In fact, recent works [5, 18-19] have highlighted that explosive modes may play a negligible role to the system's slow evolution [17–19].

Based on the TSR approach [20,21], the local stretching rate of the dynamics of a system in the direction tangential to the vector field $\boldsymbol{L}(\boldsymbol{z}) + \boldsymbol{g}(\boldsymbol{z})$, can be given by Eq. 3:

$$\omega_{\tau,pde} = \sum_{i=M}^{N+1} W_{i,pde} \lambda_i \tag{3}$$

with λ_i being the eigenvalue of the i-th mode, $W_{i,pde}$ the weight of each CSP mode defined by $W_{i,pde} = \frac{h^i}{L+g} \sum_{k=M}^{N+1} \frac{h^k}{L+g}(\boldsymbol{\alpha_k \alpha_i})$, and L+g is the norm of the vector field. Thus, it can be concluded that $\omega_{\tau,pde}$ is a linear combination of the timescales of the chemical system and it represents the stretching rate along the unit vector aligned with the state evolution direction due to the reactive-transport system. In case transport is ignored ($\boldsymbol{L}(\boldsymbol{z}) = 0$), TSR ($\omega_\tau$) is the stretching rate along the unit vector oriented in the direction of the chemical source term exclusively.

The contribution of each of reaction to the time scale ($\tau_n = 1/|\lambda_n|$) of the n-th mode can be assessed through the Time scale Participation Index (TPI) [22]. Additionally, the Amplitude Participation Index (API) measures the relative contribution of the k-th process (reaction or transport term) to the amplitude h^n of the n-th mode [23, 24]. On the basis of the API, Valorani et al. introduced the TSR Participation Index $H_k^{\omega_{\tau,pde}}$, which is a weighted sum of the API of the k-th reaction to all modes, with each weight depending on the contribution of that mode to the TSR [20, 21]. This tool provides a more generalized

view for the contribution of each process to the local evolution of the system. Therefore, the summation of all $H_k^{\omega_{\tau,pde}}$ that relate to the chemical reactions can provide a clear understanding about the role of chemical kinetics to the system's evolution. Likewise, the summation of the contributions of all the convective/diffusive terms ($H_{Conv}^{\omega_{\tau,pde}}/H_{Diff}^{\omega_{\tau,pde}}$) can clarify the role of convection/diffusion into the system and their sum ($H_{Tran}^{\omega_{\tau,pde}}$) can be used to determine the regions where transport prevails over kinetics [18, 19]. For simplicity, hereafter H_R, H_C, and H_D are used to denote the contribution of chemical, convective, and diffusive terms, respectively.

Due to the large orders of magnitude of $\omega_{\tau,pde}$, ω_τ and λ_i the logarithmic quantities of these variables will be used as follows: $\Omega_R = sign(\omega_\tau) \cdot Log_{10}|\omega_\tau|$, $\Omega_{R+T} = sign(\omega_{\tau,pde}) \cdot Log_{10}|\omega_{\tau,pde}|$, $\Lambda_i = sign(\lambda_i) \cdot Log_{10}|\lambda_i|$. It is noted that all values of $\omega_{\tau,pde}, \omega_\tau, \lambda_i < 1$ are not considered, since eigenvalues and TSR magnitudes less than unity have no meaningful impact on the system, and can be ignored. In this way, positive and negative values of Ω_R, Ω_{R+T} and Λ_i denote explosive and dissipative behavior. Furthermore, all physical time scales are normalized by a nominal time of 1 second, such that the magnitudes shown in the results are nondimensional.

3   Results and discussion

Two representative one-dimensional (1D) cases featuring a typical deflagration propagation and developing detonation transition (DDT) are selected to perform CSP and TSR analysis. A stoichiometric ethanol/air mixture at the initial base temperature and pressure conditions of T_0 of 1000 K and P_0 of 35 atm is chosen (refer to Refs. [1–3] for detailed information of the numerical schemes and configuration setup).
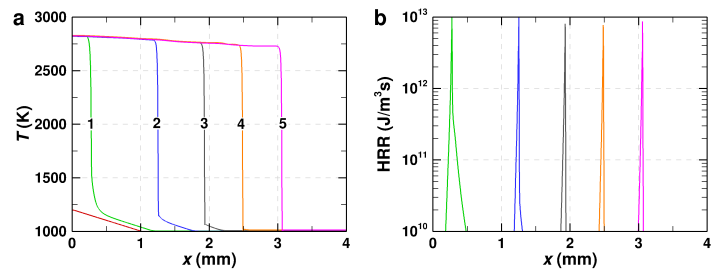

Figure 1: The spatial and temporal evolution of (a) temperature, and (b) heat release rate (HRR) for Case 1. The time sequence is numbered from 1 to 5 to denote different selected time instances.

Case 1 shown in Fig. 1 features a normal deflagration propagation. A linear hot spot with a peak temperature of 1200 K and a radius of 1 mm serves a hot spot to trigger deflagration. Once the deflagration is formed, its propagates at the speed comparable to the laminar flame speed, S_L as typically observed in SI engines. Unlike Case 1 featuring a slow speed of flame propagation, Case 2 shown in Fig. 2 features a deflagration to detonation transition (DDT) – the hot spot evolves into deflagration, gradually consuming the unburnt mixture, and finally accelerating and transiting to detonation. A highly autoignitive hot spot is initialized by a peak temperature of 2000 K and a radius of 5 mm. The hot spot is designed such that ξ ranges from 0 to 1000 within the hot spot to trigger DDT. With such a strong ignition source, as readily shown in Fig. 2, autoignition immediately forms a detonation front within the hot spot length, which is subsequently attenuated quickly upon leaving the hot spot (lines 1–4 in Fig. 2). Attributed to the low reactivity of the unburnt mixture at $T_0 = 1000$ K, HRR within the reaction zone is not fast enough to sustain a stable detonation wave propagation such that it decays quickly and transits back into deflagration at $x \sim 10$ mm. The temperature and pressure of the unburnt mixture ahead of the flame is gradually increased by the compression heating effect of deflagration (lines 5–7 in Fig. 2). With the increased reactivity of the unburnt mixture together with the flame acceleration, the deflagration front
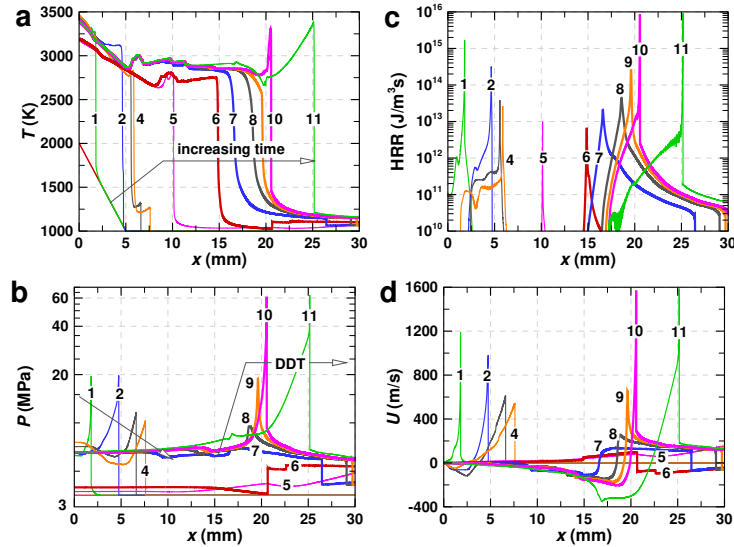
Figure 2: The spatial and temporal evolutions of (a) temperature, (b) pressure, (c) heat release rate (HRR), and (d) velocity at different time instances numbered from 1 to 11.
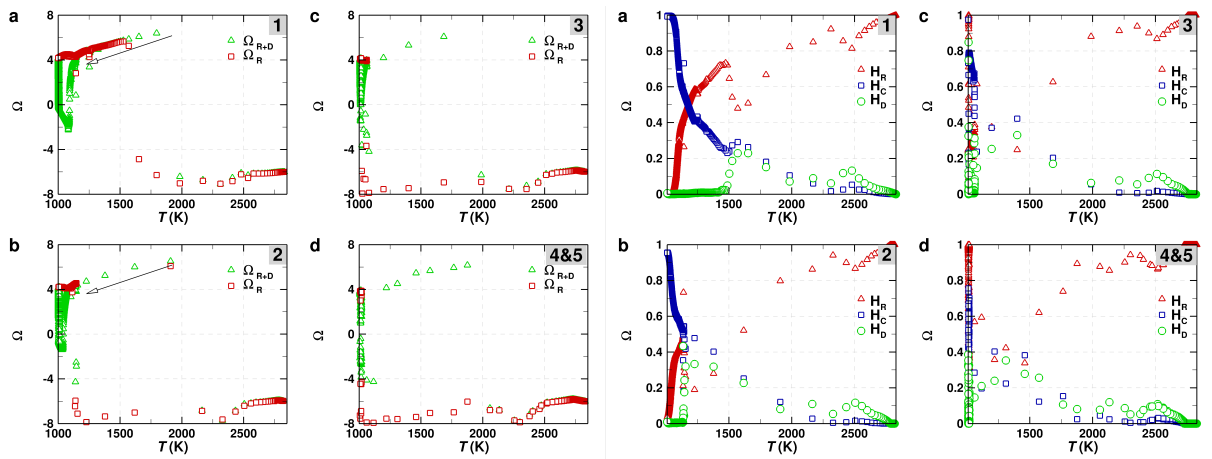

Figure 3: The evolution of TSR-API, H_R, H_C, and H_D, and the reactive/extended TSR, Ω_R and Ω_{R+D}, in the temperature space. The number in the gray box corresponds to the selected time instances shown in Fig. 1.

eventually transits into detonation at $x \sim 20$ mm and rapidly consumes the rest of the unburnt mixture (lines 8–11 in Fig. 2). Much higher pressure peaks are observed during this period. These processes are typically referred as to DDT.

The dataset of Case 1 and Case 2 are then analyzed with the CSP toolkit. The Ω_R, and the extended TSR, Ω_{R+D} together with the reaction, convection, and diffusion TSR-API, H_R, H_C, and H_D, respectively, in the temperature space at different time instances for Case 1 and 2 are shown in Figs. 3 and 4, respectively.

For Case 1 at the early time, t_1, in the location when ignition occurs (T of 1200–1500 K), both Ω_R and Ω_{R+D} are positive and nearly identical, characterizing the dominance of chemical kinetics as also depicted in the magnitude of $H_R \sim 0.6$ to 0.8 However, from t_2 to t_4, the deflagration front stably propagates, Ω_{R+D} remains positive in contrast to Ω_R that becomes negative. Ω_{R+D} accurately captures the important role of transport contributed to the explosive dynamics at the preheat zone ahead of the deflagration front for Case 1. Note that Case 1 features a laminar flame-like structure as such the
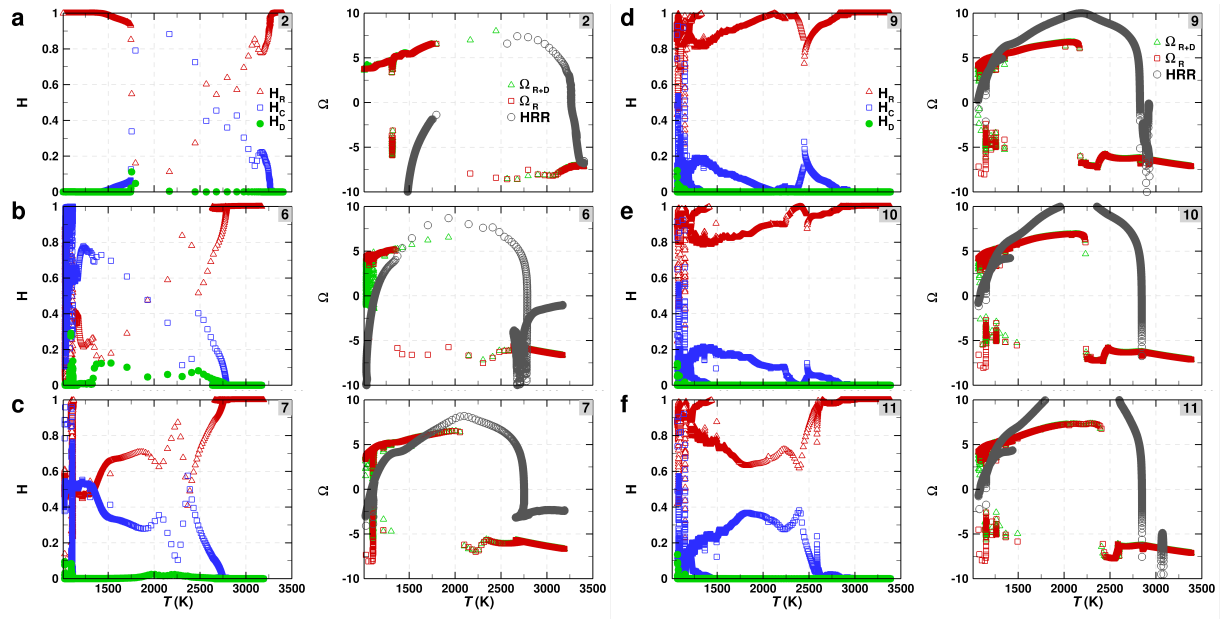
Figure 4: The evolution of TSR-API, H_R, H_C, and H_D, and the reactive/extended TSR, Ω_R and Ω_{R+D}, in the temperature space. The number in the gray box corresponds to the selected time instances shown in Fig. 2.

contribution of transport is comparable with that of chemistry in the reaction zone region. Figure 3 shows a consistent result that the value H_R representing the contribution from reaction is comparable with the sum of H_C and H_D representing the contribution from transport.

In contrast with Case 1, Case 2 exhibits a deflagration to detonation transition, characterized by a fast deflagration front eventually transited into a detonation wave as shown in Fig. 2. Case 2 with a much bigger hot spot size, $r_{hs} = 5$ mm, induces a strong pressure wave after the occurrence of the hot spot autoignition, as seen in Fig. 2 at t_1 to t_4 that significantly enhances the development of detonation development at later time. The progression of DDT in time is again well-captured by the extended TSR Ω_{R+D} and TSR-API shown in Fig. 4. Particularly, the contribution of chemical kinetics is found to be dominant throughout the DDT process. However, the contribution from transport is also found to be non-negligible, i.e., H_C from the convection term varies from 10% to 50%.

4 Conclusion

This study elucidates the thermochemical characteristics of a developing ignition process by performing computational singular perturbation (CSP) and tangential stretching rate (TSR) analysis. The relative contribution of chemical kinetics, diffusion, and convection on the progression of superknock development is identified. It is found that in addition to the dominant contribution of chemical kinetics, the contribution of transport in triggering the developing detonation transition (DDT) is non-negligible, i.e., ranging approximately from 10% to 50% in the preheat zone where the DDT occurs.

Acknowledgments

Sapienza University of Rome for providing the CSP toolkit.

References

[1] M. B. Luong, H. G. Im, Direct numerical simulation of preignition and knock in engine conditions, in: A. S. K. A. R. A. Gupta A.K., De A. (Ed.), Advances in Energy and Combustion: Green Energy and Technology, Springer, 2022, pp. 311–336. doi:10.1007/978-981-16-2648-7_14.

[2] M. B. Luong, S. Desai, F. E. Hernández Pérez, R. Sankaran, B. Johansson, H. G. Im, A statistical analysis of developing knock intensity in a mixture with temperature inhomogeneities, Proc. Combust. Inst. 38 (2021) 5781–5789.

[3] M. B. Luong, S. Desai, F. E. Hernández Pérez, R. Sankaran, B. Johansson, H. G. Im, Effects of turbulence and temperature fluctuations on knock development in an ethanol/air mixture, Flow Turbul. Combust. 106 (2021) 575–595.

[4] S. Desai, J. K. Yu, W. Song, M. B. Luong, F. E. Hernández Pérez, R. Sankaran, H. G. Im, Direct numerical simulations of reacting flows with shock waves and stiff chemistry using many-core/GPU acceleration, Computers & Fluids 215 (2021) 104787.

[5] Z. Wang, H. Liu, R. D. Reitz, Knocking combustion in spark-ignition engines, Prog. Energy Combust. Sci. 61 (2017) 78–112.

[6] Gautam T Kalghatgi, Derek Bradley, Pre-ignition and 'super-knock' in turbo-charged spark-ignition engines, Int. J. Engine Res. 13 (2012) 399–414.

[7] M. Figueroa-Labastida, M. B. Luong, J. Badra, H. G. Im, A. Farooq, Experimental and computational studies of methanol and ethanol-preignition behind reflected shock waves, Combust. Flame 234 (2021) 111621.

[8] Y. B. Zeldovich, Regime classification of an exothermic reaction with nonuniform initial conditions, Combust. Flame 39 (1980) 211–214.

[9] X. Gu, D. Emerson, D. Bradley, Modes of reaction front propagation from hot spots, Combust. Flame 133 (2003) 63–74.

[10] M. B. Luong, F. E. Hernández Pérez, H. G. Im, Prediction of ignition modes of NTC-fuel/air mixtures with temperature and concentration fluctuations, Combust. Flame 213 (2020) 382–393.

[11] M. B. Luong, F. E. Hernández Pérez, A. Sow, H. G. Im, Prediction of ignition regimes in DME/air mixtures with temperature and concentration fluctuations, AIAA SciTech 2019 Forum (2019) https://doi.org/10.2514/6.2019–2241.

[12] M. J. M. Ali, M. B. Luong, A. Sow, F. E. Hernández Pérez, H. G. Im, Probabilistic approach to predict abnormal combustion in spark ignition engines, SAE paper (2018) 2018–01–1722.

[13] S. Lam, D. Goussis, Understanding complex chemical kinetics with computational singular perturbation, in: Proc. Combust. Inst., Vol. 22, Elsevier, 1989, pp. 931–941.

[14] D. A. Goussis, H. G. Im, H. N. Najm, S. Paolucci, M. Valorani, The origin of cema and its relation to csp, Combust. Flame 227 (2021) 396–401.

[15] E.-A. Tingas, D. C. Kyritsis, D. A. Goussis, H2/air autoignition dynamics around the third explosion limit, J. Energ. Engineer. 145 (1) (2019) 04018074.

[16] E.-A. Tingas, Computational analysis of the effect of hydrogen peroxide addition on premixed laminar hydrogen/air flames, Fuel 302 (2021) 121081.

[17] Y. J. Kim, W. Song, F. E. H. Pérez, H. G. Im, Explosive dynamics of bluff-body-stabilized lean premixed hydrogen flames at blow-off, Proc. Combust. Inst. 38 (2) (2021) 2265–2274.

[18] D. M. Manias, E.-A. Tingas, F. E. H. Pérez, R. M. Galassi, P. P. Ciottoli, M. Valorani, H. G. Im, Investigation of the turbulent flame structure and topology at different karlovitz numbers using the tangential stretching rate index, Combust. Flame 200 (2019) 155–167.

[19] D. M. Manias, E.-A. Tingas, Y. Minamoto, H. G. Im, Topological and chemical characteristics of turbulent flames at mild conditions, Combust. Flame 208 (2019) 86–98.

[20] M. Valorani, S. Paolucci, E. Martelli, T. Grenga, P. P. Ciottoli, Dynamical system analysis of ignition phenomena using the tangential stretching rate concept, Combust. Flame 162 (8) (2015) 2963–2990.

[21] M. Valorani, P. P. Ciottoli, R. M. Galassi, Tangential stretching rate (tsr) analysis of non premixed reactive flows, Proc. Combust. Inst. 36 (1) (2017) 1357–1367.

[22] D. A. Goussis, H. N. Najm, Model reduction and physical understanding of slowly oscillating processes: the circadian cycle, Multiscale Modeling & Simulation 5 (4) (2006) 1297–1332.

[23] J. Prager, H. N. Najm, M. Valorani, D. Goussis, Structure of n-heptane/air triple flames in partially-premixed mixing layers, Combust. Flame 158 (11) (2011) 2128–2144.

[24] M. Valorani, H. N. Najm, D. A. Goussis, Csp analysis of a transient flame-vortex interaction: time scales and manifolds, Combust. Flame 134 (1-2) (2003) 35–53.